

Article

Effect of CH₄–Air Ratios on Gas Explosion Flame Microstructure and Propagation Behaviors

Xianfeng Chen *, Yin Zhang and Ying Zhang

School of Resource and Environment Engineering, Wuhan University of Technology, Wuhan 430070, China; E-Mails: chexfox@gmail.com (Y.Z.); samuelying@foxmail.com (Y.Z.)

* Author to whom correspondence should be addressed; E-Mail: cxf618@whut.edu.cn; Tel.: +86-27-8765-1816; Fax: +86-27-8765-4177.

Received: 18 August 2012; in revised form: 24 September 2012 / Accepted: 18 October 2012 / Published: 22 October 2012

Abstract: To reveal the inner mechanism of gas explosion dynamic behavior affected by gas equivalent concentration, a high speed Schlieren image system and flow field measurement technology was applied to record the gas explosion flame propagation and flame structure transition. The results show that a flame front structure transition occurs, followed by a flame accelerating propagation process. The laminar to turbulence transition was the essential cause of the flame structure changes. The laminar flame propagation behavior was influenced mainly by gas expansion and fore-compressive wave effect, while the turbulent flame speed mostly depended on turbulence intensity, which also played an important role in peak value of the explosive pressure and flame speed. On the condition that the laminar-turbulent transition was easier to form, the conclusion was drawn that, the lowest CH₄ concentration for maximum overpressure can be obtained, which was the essential reason why the ideal explosive concentration differs under different test conditions.

Keywords: gas concentration; gas explosion; flame structure; propagation behavior

1. Introduction

It is well known that methane gas has become one of the most important alternative fuels, that is found hidden in coal seams in an adsorption state. Nowadays it is widely used as a civil fuel, industrial fuel, power generation fuel, automobile fuel and chemical raw material, to which great attention has been paid by almost all the countries in the World. However, should the gas be released or an

explosion occur during the storage or transport process, destruction to the ecological environment and people could occur. To prevent gas explosions, therefore, lots of scholars have carried out exhaustive explorations of the explosive limit range and characteristic detonation dynamics and influencing factors [1–6]. Studies show that the equivalence ratio is one of primary factors affecting the process and characteristics of CH₄ gas combustion and explosions, which influences the flame propagation behavior and the flow field structure through the chemical reaction and the energy release process steps, such as flame acceleration, flame structure and instability and flow behavior [7–11].

The explosion pressure rises sharply, which is directly caused by the flame acceleration. Generally due to the hydrodynamic instabilities the flame propagates as a curved front rather than maintaining a stable planar front [12]. Clanet and Searby [13] first explained the acceleration mechanism at the early stages of burning in tubes, and the idea was recently developed by Bychkov's theory [14]. According to the acceleration mechanism, acceleration happens due to the initial ignition geometry in the tube axis when a flame develops into a finger-shaped front, with surface area growing exponentially in time. Flame surface area grows quite fast, but only for a short time. Many studies found that obstacles or chamber size change may enhance the laminar-turbulent flow transition [1,3,15,16]. According to Shelkin turbulent combustion theory [17], turbulence plays an important role in the combustion process and flame acceleration behavior, and further increases the explosion pressure. Shelkin first explained the flame acceleration in tubes with slip walls. The Shelkin mechanism involved thermal expansion of the burning gas, non-slip at the tube walls and turbulence as the main components of flame acceleration. When a flame propagates from a closed tube end, the burning gas expands and pushes a flow of the fuel mixture. The flow becomes strongly non-uniform because of non-slip at the walls. The non-uniform velocity distribution makes the flame shape curved, which increases the burning rate and drives the acceleration. Turbulence provides additional distortion of the flame front and compensates for thermal losses to the walls. Another flame acceleration mechanism induced by obstacles was developed by Bychkov [18]. Bychkov's mechanism is qualitatively different from the Shelkin's mechanism as it provides ultrafast flame acceleration independent of the Reynolds number. The Bychkov mechanism states that flame acceleration happens due to a jet-flow in the free channel part driven by the delayed burning between the obstacles. Recently, an analytical theory of accelerating flames has also been developed for a two dimensional tube geometry with one end closed and nonslip at the walls by Akkerman *et al.* [19]. The quantitative theory and modeling of Shelkin's mechanism was first studied by Bychkov [20]. They considered laminar premixed flames with a realistically strong density drop at the front. The most important features of flame acceleration have been obtained analytically, such as the exponential regime of the flame acceleration, the acceleration rate, and the self-similar flame shape. The non-uniform velocity distribution makes the flame shape curved, which increases the burning rate and drives the acceleration. It was also shown that flame front instability generated by the interaction between the flame and a pressure wave causes rapid flame acceleration. Some researchers found that lower pressures can be expected because of the relative proximity of the vent to obstacles in the building, the larger eddies allow for increased flame area deformation, and hence increased burning rates and higher pressures [21–23].

Some researchers have discovered that the initial turbulence enhanced the combustion reaction rate and heat and mass transfer efficiency [24–27], and enlarged the range of the explosive concentration limit. Fundamental and thorough investigation of equivalence ratios effect on flame microstructure and

propagation behavior has not been performed yet, even though some studies regarding hydrogen fires have been recently conducted [28]. Studies of premixed flames in a compartment are required to understand the fundamental characteristics of equivalence ratio effect on flame propagation behavior and improve the safety of the burning process.

In the present paper we demonstrate the explosion flame structure characteristics and dynamic behavior, and reveal the relationship between different equivalence ratios and gas explosion dynamic behavior, which aims to provide theoretical and experimental guidance for preventing and controlling gas explosion disasters.

Over the last decade, progress within the field of optical diagnostics has produced tools that can provide data containing high levels of both spatial and temporal resolution [29]. These tools have allowed sequences of flame images, flame speed profiles and turbulence characteristics to be measured without disturbing the interactions being investigated. High-speed Schlieren image technology was one of the most applicable techniques for characterizing the flame–flow interaction and flame propagation behavior. Through Schlieren images, the progression of the propagating flame is captured, thus obtaining qualitative information about flame shape and scales of flame front wrinkling [3,30,31]. Wu studied the flame acceleration of stoichiometric ethylene/oxygen mixtures in microscale tubes and clearly observed the DDT behavior using a high-speed CCD camera [32]. Therefore, the high speed Schlieren image system and dynamic testing technology were applied in the experimental test of premixed gas explosions and flame propagation. The experimental system was established to record the flow characteristics and dynamic behavior of gas explosions in a semi-vented pipe, and to reveal the influencing rules and intrinsic mechanism of explosion flames at different equivalence ratios.

2. Results and Discussion

2.1. Flame Structure Characteristic Based on High Speed Schlieren Photographs

As well known, the change of flow field density shows the influences of temperature, concentration and flow field pressure on the flame structure. The Schlieren image method is based on the light refraction of flow, therefore, can be used to reflect the inner flow structure characteristics directly. The process of laminar-turbulent transition and the inner characteristics of flame fields can be recorded clearly by the Schlieren image technology [33].

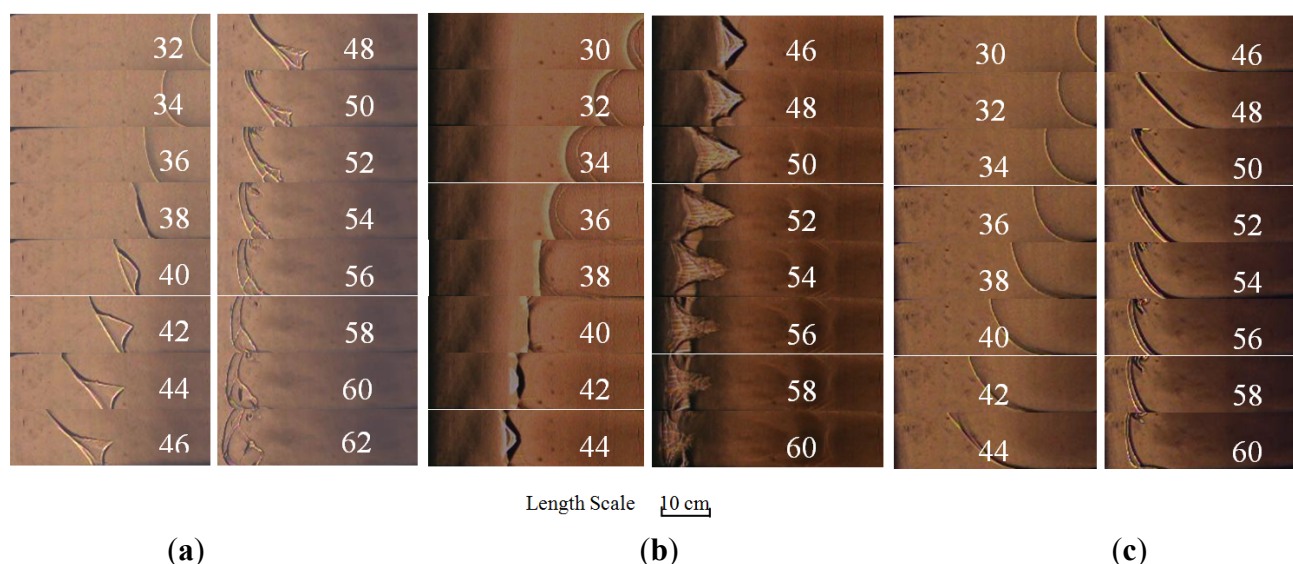
Figure 1b shows a section of typical high speed Schlieren images of flame propagation at the chemical equivalence ratio (volume concentration 9.5%). In the initial stage, the flame fronts spread in an obviously laminar regime. Still, at the time instant of about $t = 42$ ms, the flame structures changed remarkably and we observed development of the “V” flame shape, referred typically as the “tulip flame” structure [34]. After that the flame front was gradually stretched while the reaction zone became thicker than that of the laminar flame, which indicated that the turbulent flame structure began to appear. According to gas combustion theory, just at this point did the reaction efficiency and heat release rate get greatly enhanced, which would help to speed up flame propagation and the laminar-turbulent transition [14,35]. Different explanations have been provided for the mechanism of flame instability and tulip flame formation by theories such as the Taylor-Markstein instability [36], the Darrieus-Landau dynamic instability [37] and the pressure-flame interaction instability theory [38]. The current study is

also conceptually close to the work of Zeldovich and Bychkov [14]. The local acceleration starts when the flame evolves from a hemispherical kernel to the finger-shaped front of Figure 1; the acceleration stops when the flame skirt touches the wall. In the present paper the flame acceleration occurs in the early stages of burning in tubes with slip walls, as proposed by Clanet and Searby [13]. Bychkov demonstrated that the flame surface area increases approximately by a factor of 15–20 in comparison with the tube cross section because of acceleration. In the present paper the acceleration of premixed laminar flames in tubes is in good agreement with the mechanism suggested in [13]. Acceleration happens due to the initial geometry of flame ignition, when a flame develops from a spherical kernel to a finger shaped front. The result from our research showed that the flame front structure changed along with flow field characteristics [31]. The small-scale vortex enhanced the heat and mass transfer and thickened the flame fronts, while the large-scale vortex tended to cause flame structure instability during the laminar-turbulent transition process.

The high-speed Schlieren images for a volume concentration of 8% are shown in Figure 1a. In the initial stage, the flame front has a symmetrical spherical structure which represents typical laminar flow. After $t = 34$ ms, the flame front structure became asymmetric as the upper flame speed exceeded the lower one. At $t = 40$ ms, the flame front was torn into an asymmetric tulip flame structure.

Figure 1c clearly shows the process of flame propagation at an equivalence concentration of 11%, as revealed by the Schlieren images of the flame propagation behavior. The flame propagated forward as regular laminar flame in the initial stage, and as it developed and propagated, the flame structure became increasingly inclined severely but a tulip flame was not generated.

Figure 1. High speed Schlieren images of flames at different volume concentrations: (a) 8%, (b) 9.5%, (c) 11%.



Based on the discussion on the CH₄–air flame structure above, it can be seen that, the equivalence ratio plays an important role in flame microstructure. In the case of chemical equivalence ratio (the equivalence ratio is 1.0 for a CH₄ equivalence concentration 9.5%), the flame structure was symmetrical all the time, and the whole process of tulip flame structure evolution was clear, while under the other conditions—either rich fuel (equivalence concentration 11%) or lean fuel (equivalence

concentration 8%)—the flame structure became irregular and asymmetrical. Patnaik *et al.* and Bychkov *et al.* have suggested that the asymmetrical flame structure is mainly caused by the influence of buoyancy [39–41]. The Froude number is a dimensionless number defined as the ratio of the inertia to gravitational forces:

$$Fr = V^2/gL \quad (1)$$

where V is the speed of flame, g is the acceleration due to gravity, and L is the characteristic length of the tube (in our paper, it was chosen as the side length of the cross-section). For the rich fuel or lean fuel conditions, the flame speed is small and the buoyancy plays an important role in flame structure. In our experiments, at the stage of flame structure change (where the mean flame speeds were much smaller), the Froude numbers were 0.22 and 0.68 for the concentrations of 8% and 11%, respectively, which were much smaller than the unit. That means the influence of buoyancy is important when the concentrations are 8% and 11%, so the flame structure becomes irregular and asymmetrical. For the case of 9.5% (the equivalence ratio is 1.0), the flame speed is much larger and the influence of buoyancy becomes very small, and therefore the flame looks symmetrical.

Bychkov considered that the flame instability in this case is often accompanied by mass flux through the unstable interface, which may have either a stabilizing or a destabilizing influence, and is mainly due to the Darrieus–Landau instability of a flame front [42].

To understand the flame dynamics and flame structure clearly, some researchers (Davis *et al.* [43], Akkerman and Bychkov [44], *et al.*) have provided detailed data and results on the inner mechanism of laminar flame structure change, such as the laminar flame velocity, the effective flame thickness, the ratio of the unburnt to burnt gas density and the effective Markstein number. The relevant dynamic parameters in Table 1 can be used as a reference to describe the flame dynamics and flame structure [42]. Markstein numbers of the flames manifests the linear relationship between the local burning velocity and the local curvature. As shown in Table 1, the values of Markstein number relative to the unburned and burned gases are not equal with different mixture concentrations, therefore the flame stretch rates were also different due to different equivalence ratios.

Table 1. Flame dynamic parameter from [42].

equivalence ratio	volume concentration	s_u^o (cm/s)	δ (cm)	ρ_u/ρ_b	Ma
0.80	7.6%	25.4	0.009	6.65	4.69
0.90	8.6%	32.5	0.225	7.12	5.54
1.00	9.5%	37.1	0.217	7.48	6.20
1.10	10.5%	38.3	0.225	7.55	6.99
1.20	11.4%	34.5	0.215	7.43	7.96
1.30	12.4%	25.0	0.291	7.28	9.13

s_u^o is laminar burning velocity, δ is flame thickness, ρ_u/ρ_b is the density ratio of unburnt and burnt gas, Ma is Markstein number.

2.2. Flame Propagation Behavior on Different Equivalence Ratios

Figure 2 shows the history of flame speed and pressure *versus* time at different equivalence ratios. Here, the flame speed was defined and measured as the velocity of the flame tip in the laboratory reference frame. The flame speed takes into account the intrinsic propagation of the flame front and drift of the flame with the flow. Based on the high speed Schlieren photographs of flame front position with time, the flame front tip position and the relevant time can be discerned, then the flame speed can be calculated.

Figure 2. Relationship between flame speed and pressure with time: (a) volume concentration: 11%; (b) volume concentration: 9.5%; (c) volume concentration: 8%.

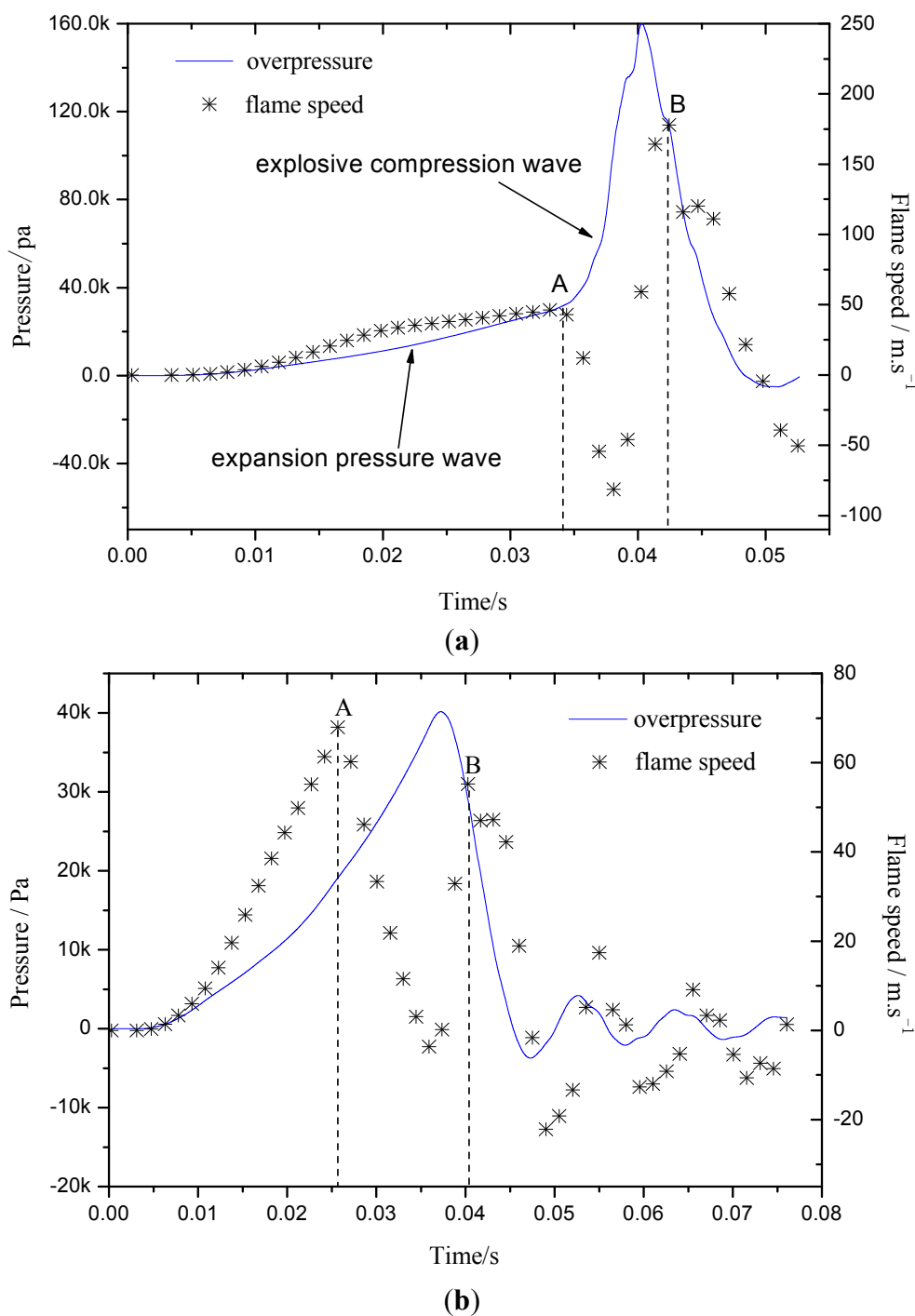
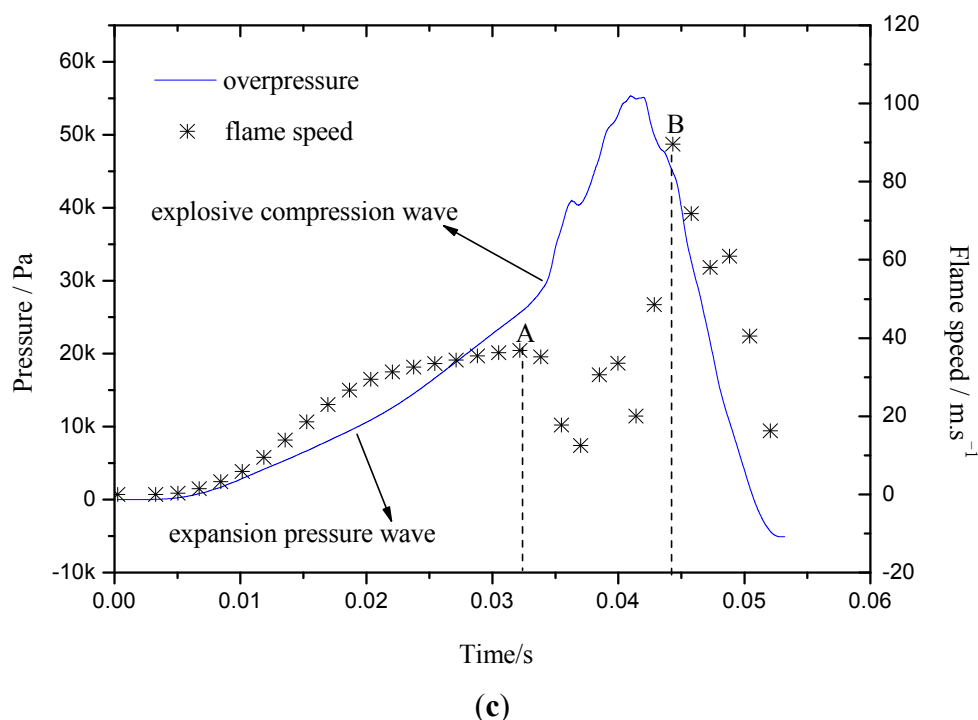


Figure 2. Cont.



Especially for the laminar flame, the flame front was regular and smooth, so the laminar flame speed was easy to obtain, while for the turbulent flame, due to the vortex characteristics and the irregular flame front profile, it is more complicated than the laminar case to discern the flame tip position. In this case, we can trace one point or one part of the flame front as the “flame tip”, based on the “flame tip” position and time, then the local flame speed can be also calculated and obtained instantaneously.

When the equivalence ratio is 9.5%, the flame speed increased gradually after ignition, and the curve reached the peak value at $t = 25.7$ ms. After then the flame speed began to drop, accompanied with a vast fluctuation caused by the reflected pressure wave. It was just the reflected pressure wave that induced the laminar-turbulent transition and fierce flow field perturbation, and made the flame speed further fluctuate sharply, even with the instantaneous reverse direction speed. Research showed that the co-current pressure wave helps to accelerate flame propagation, but the reverse pressure wave suppresses flame-propagation [45]. Therefore, it can be deduced that the flame speed fluctuation in Figure 2 was determined mainly by the turbulence intensity, and the process of flame speed fluctuation ($t = 26\sim 45$ ms) can be also used to represent the change stage of flame flow field structure from the high speed Schlieren photographs (Figure 1), which further proved that the laminar-turbulent transition caused the flame speed fluctuation directly. The flame speed curves demonstrate a similar trend based on a different equivalence ratio.

According to the curve, the flame speed reached the first peak value at the laminar flame stage and then the speed fluctuated, which finally led to the maximum flame speed in the process of flame propagation. In Figure 2a,c, we cannot observe any pulsations in the flame speed, but only one or two pressure beats, which are related, probably, to shock waves reflected from the tube end. In Figure 2b the pulsations are obvious, but they are quite regular, which discards the possibility of turbulent origin for the pulsations. Some studies by Bychkov *et al.* [46] and Petchenko *et al.* [47] show that flame interaction with the sound waves may also lead to important flame dynamics effects. Thus, we deduced

that these pulsations in Figure 2 may be related to the sound waves generated by the flame front in the closed tube. The characteristic acoustic time of the chamber (time for a round trip) is $\tau = 2L/c$ (L is the tube length, c is the local sound velocity). This is of the order of $\tau = 11.4$ ms for a mean sound speed of 350 m/s, and 8 ms for a mean sound speed of 500 m/s. So, in a period of 8 ms, the compressive wave has already made a round trip of the chamber and interacted twice with flame fronts, finally the interaction of sound waves on flame leads to the fluctuation of the dynamic behavior in Figure 2.

Figure 2 showed that the flame speed and acceleration rate and the pressure increased slowly at the beginning of flame propagation, due to the typical laminar burning [48]. The flame propagation in the early stage was mainly influenced by the burnt gas expansion pressure ($t < t_A$). Before the flame speed rose up to the first peak, the history of flame speed-time was in agreement with the exponential law and the trend was similar to the flame growth rate in Bychkov's work [14]. While the value in present study was larger than that in Bychkov's work, the differences may be caused mainly by the initial test conditions such as pipe scale and ignition energy and the restriction conditions. When it reached the first peak value ($t = t_A$), the flame speed dropped sharply, accompanied by fluctuations. After then the pressure increased rapidly, which was mainly caused by the superposition of compressive pressure (shock wave) and the reflected pressure wave. Meanwhile, the flame speed declined due to the counter flow induced by the reflected pressure wave. Moreover, the interaction of reflected pressure wave and flame flow hastened the laminar-turbulent transition. Once the turbulence intensity became strong enough, the flame speed would rise sharply and reach a second peak at time $t = t_B$. Generally, at the second peak point B, the flame speed became much larger than that of laminar flame. Under the condition of 9.5% equivalence concentration, the peak speed of the laminar flame reached 38 m/s at the moment t_A but not at t_B , where the reason was that less laminar-turbulent transition was finished in that case, and the turbulent burning was not strong enough. Compared with the flame speed and pressure of different equivalence ratios, the peak speed ($t = t_A$) occurred in the laminar stage on the case of 9.5% equivalence concentration, while other peak speeds were obtained in the turbulent burning stage ($t = t_B$). In the case of 11% equivalence concentration, the fluctuation range of flame speed was most substantial in accord with the biggest turbulence intensity, and the maximum explosion pressure was also obtained.

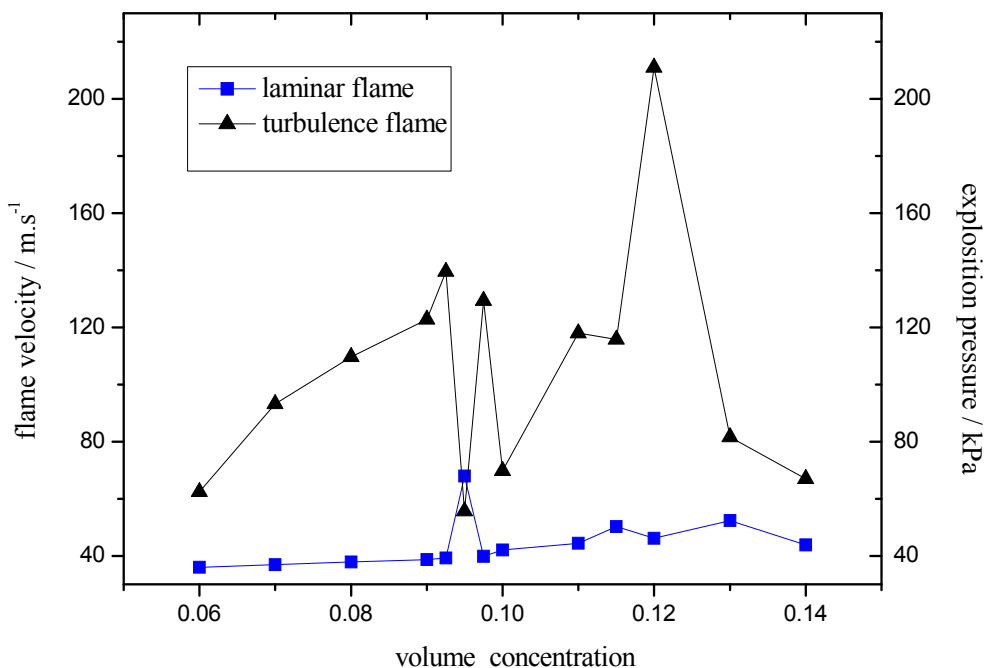
From Figure 2, it can be seen that the flow Mach number approaches unity in the present experiments, where the effects of gas compressibility become of importance. The role of gas compressibility in flame acceleration was studied by Bychkov *et al.* [49–51]. They demonstrated that gas compression moderates flame acceleration in channels by measuring the Mach number of the flow. Moderation was described as a combination of linear and nonlinear effects. The linear effect reduces the rate of exponential flame acceleration with initial Mach number at the very beginning of the process, while the nonlinear effect becomes important as the flame moves away from the closed tube end.

2.3. The Flame-Propagation Dynamics Characteristic on Different Flow Structure

As known to all, flame propagation in a pipe always goes through the laminar and turbulent burning phase. To reveal the gas explosion dynamic characteristics influenced by gas volume concentration, the laminar flame speed and the subsequent turbulent speed are described in Figure 3.

As shown in Figure 3, the maximum speed of the laminar flame was obtained in the case of 9.5% volume concentration, while that of turbulent flame was found at 12% concentration. Generally, the turbulence speed was bigger than the laminar one, but the laminar flame speed was smaller than the turbulent speed in the case of 9.5% volume concentration, mainly due to the weaker turbulence intensity.

Figure 3. Flame velocity vs. volume concentration.



The relationship between the peak flame speed and explosive pressure of different flow structure was shown in Figures 4 and 5, respectively.

Figure 4. Explosion pressure and flame speed in the laminar stage.

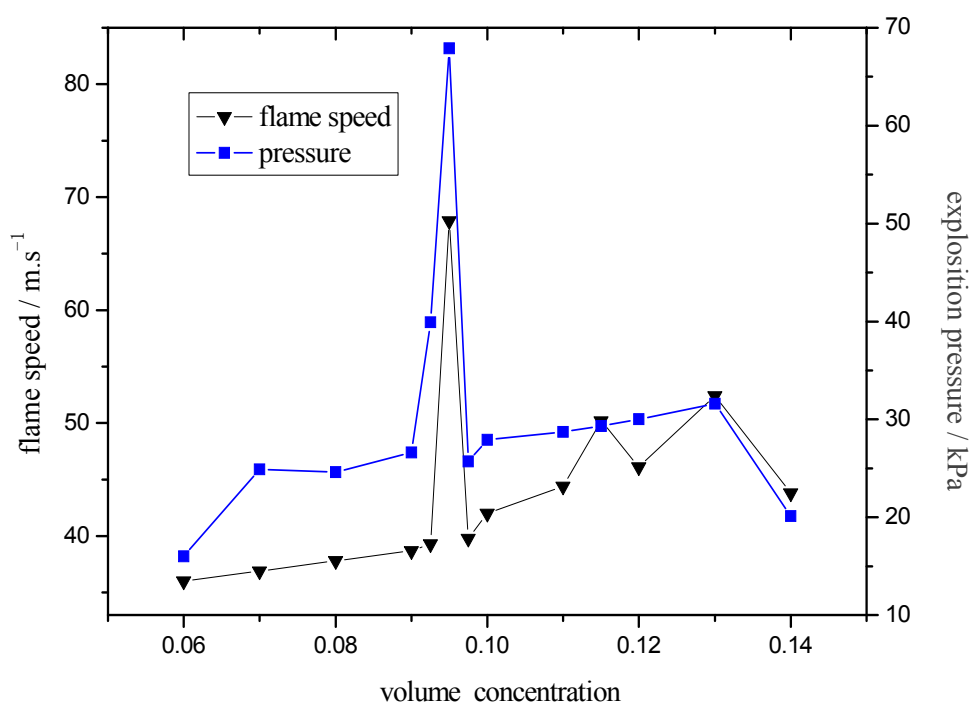


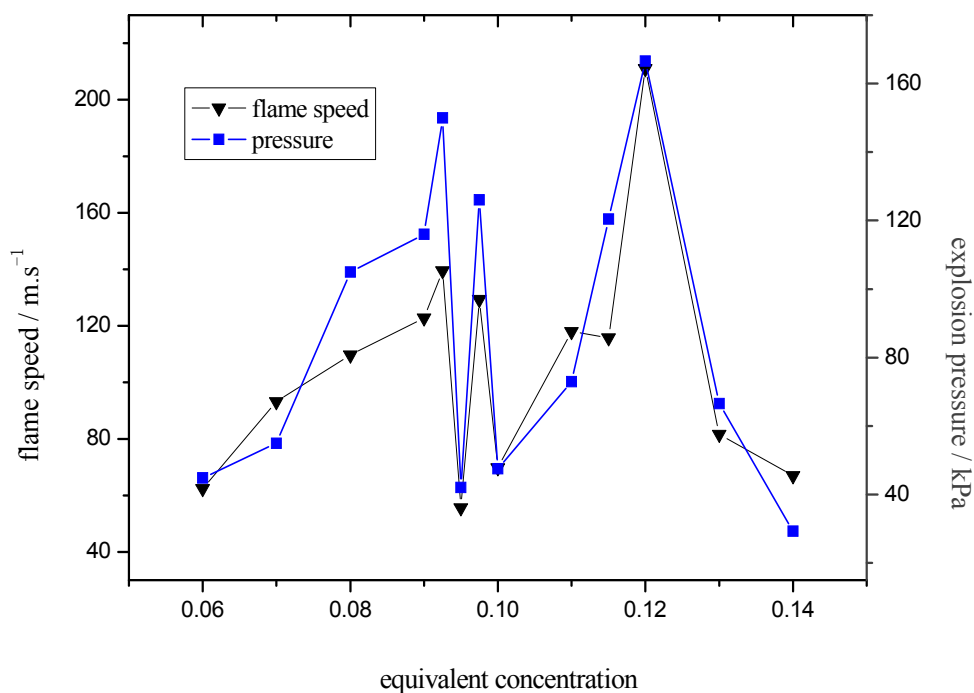
Figure 5. Explosion pressure and flame speed in the turbulent stage.

Figure 4 shows the curves of laminar flame speed and explosion pressure in the case of the CH₄ concentration range from 6% to 14%. In the laminar burning stage, the results showed that, both the flame speed and explosion pressure rose up to the peak value at the chemical equivalent concentration (9.5%), while as shown in Figure 5, the pressure and flame speed (the second peak of flame speed, caused by turbulent flow as shown in Figure 2) were minimum at the optimum chemical concentration (9.5%), which means that the laminar-turbulent transition was not completed in such a case. The experiment result in Figure 5 show that, the maximum explosion pressure was easier to reach in the condition of lean fuel or rich fuel than of the optimum chemical concentration (9.5%) which was once considered to be most liable to reach the maximum explosion pressure. The research also shows the flame speed and explosion pressure up to a maximum value at about 12% concentration. According to gas explosion theory, explosion pressure rises due to the flame accelerating directly. It was just the flame acceleration that brought about the explosion pressure. As shown in Figures 4 and 5, the pressure and speed curve changing trends are similar, which matches the gas explosion theory very well.

The maximum explosion pressure and flame speed were obtained not on the condition of optimum chemical concentration, mainly due to the incomplete laminar combustion and two-stage reaction process, and so on. Under the conditions of a volume concentration 11%, it takes 8 ms (from t_A to t_B) for the flame to accomplish laminar-turbulent transition. At a volume concentration of 8%, the laminar-turbulent transition time lasts 12 ms, while at a volume concentration of 9.5%, it takes more than 15 ms to accomplish the laminar-turbulent transition. Compared with the case of 9.5%, it's much easier to form laminar-turbulent transition at about 11%. It can be seen that near the concentration point where it is easier to form the laminar-transition, much larger peak pressure and flame speed can be obtained. Therefore, the optimum explosion concentration can be reached.

In this experiment, the optimum explosion concentration of methane is 12%, larger than the value 11% in the research [52]. The mainly reason was that, the maximum explosion pressure and velocity both

occurred in the turbulence stage, where the flame speed was influenced mainly by turbulence effects. Therefore, the turbulence intensity was vital to the maximum explosion pressure and flame speed. Besides, different experimental systems and conditions also played important roles in laminar-turbulent transition and turbulence intensity. Compared with the straight pipe in the experiment, the spherical container in the research was more helpful to hasten the laminar-turbulent transition, and therefore it was easier to reach the optimum concentration.

3. Experimental Section

3.1. Experimental Apparatus

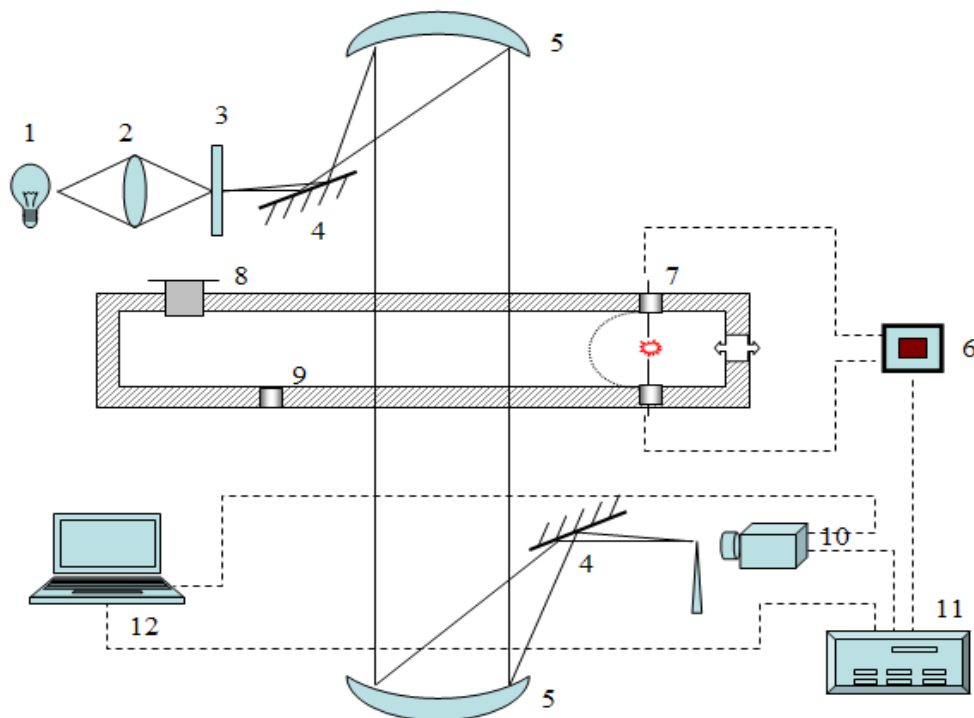
The experiment was performed on a premixed gas explosion and propagation behavior platform. The structure of the experimental system was shown in Figure 6, and mainly consists of a combustion pipe, a data acquisition system, a high speed camera system, a Schlieren image system and an ignition system. The Schlieren image system was composed of a 25 W halogen tungsten lamp, two concave mirrors with focal length 3 m, a focusing lens and a knife edge. The pipe was placed horizontally and the cross section of combustion pipe was square with the inner size 60 mm × 60 mm × 2,000 mm. The two sides of the pipe were made up of high strength optical glass for observation of the dynamic process of flame propagation. The pressure relief valve was set on the right end of the pipe to ensure the experimental system safety when overpressure rose to some extent. The ignition electrode was set up 5 cm from the right end. When ignited, the flame propagates from right to left in the pipe. The flame structure and dynamical characteristics were caught by the high frequency dynamic pressure sensor in the center of the pipe and high speed Schlieren image system.

3.2. Experimental Procedure

The experimental system was set up according to Figure 6. Before the test, the combustion pipe was evacuated by vacuum pumping, and then filled with premixed methane/air at a certain equivalence ratio. Meanwhile the relief valve was covered with 0.2 mm thick PE film on the right pipe. When an electric spark ignited the premixed gas, the high speed Schlieren system and pressure sensor would record the flame front structure and propagation behavior. The high voltage igniter, high speed camera system (Fastcam SA1.1, Photron Company, Tokyo, Japan) and data acquisition system (8826 Memory Recorder, HIOKI Company, Nagano, Japan) were set up to go into operation at the same time by a synchronization controlling device. The specific conditions of the experiments were as follows:

- Methane volume concentration: 6%–14%;
- Ignition voltage: 30,000 V;
- Ignition time: 0.01 s;
- High speed camera meter frequency: 10,000 shooting frame/s;
- Data sampling frequency: 100 kHz.

Figure 6. Sketch of gas explosive experiment system: (1) halogen tungsten lamp; (2) convex lens; (3) slit; (4) reflecting mirror; (5) concave mirror; (6) spark igniter; (7) ignition electrode; (8) discharge vent; (9) pressure sensor; (10) high speed video camera; (11) synchronization controller; (12) computer.



4. Conclusions

Experimental studies have been carried out to investigate the gas explosion flame propagation and flow structure transition. Based on the discussions, the conclusions were drawn as following:

- (1) The flame front structure transition was closely connected to the flame acceleration propagation process and flow character. The flame structure change was mainly due to the flow transition from laminar to turbulent.
- (2) The explosion flame was divided into laminar and turbulent stages. At different flame stages, the factors influencing flame propagation were different. The laminar flame propagation behavior was influenced mainly by gas inflation and pressure wave effects, while the turbulent flame speed was greatly dependent on turbulence intensity.
- (3) The turbulence intensity played an important role in peak value of explosive pressure and flame speed. On the case that it's easier to form laminar-turbulent transition, the ideal explosive concentration would be easier to reach, which was the essential reason why the ideal explosive concentration differs under different test conditions.

Acknowledgments

This work was supported by the National Natural Science Foundation of China (No. 51174153 and No. 50804038) and Open Project of State Key Laboratory of Fire Science (HZ2011-KF06) and the Fundamental Research Funds for the Central Universities (2012-II-011).

References

1. Masri, A.R.; Ibrahim, S.S.; Nehzat, N. Experimental study of premixed flame propagation over various solid obstructions. *Exp. Therm. Fluid Sci.* **2000**, *21*, 109–116.
2. Craig, T.; Johansen, G.C. Visualization of the unburned gas flow field ahead of an accelerating flame in an obstructed square channel. *Combust. Flame* **2009**, *156*, 405–416.
3. Fairweather, M.; Hargrave, G.K.; Ibrahim, S.S. Studies of premixed flame propagation in explosion tubes. *Combust. Flame* **1999**, *116*, 504–518.
4. Alexiou, A.; Andrews, G.E.; Phylaktou, H. Side-vented gas explosion in a long vessel: The effect of vent position. *J. Loss Prev. Process Ind.* **1996**, *5*, 351–356.
5. Yang, Y.; He, X.Q. Fractal characteristics of flame front surface in premixed turbulent methane/air combustion. In *Proceedings of 5th International Autumn Seminar on Propellants, Explosives and Pyrotechnics*, Guilin, China, 15–18 October 2003.
6. Yang, Y. The Flame Microstructure of Gas Explosion and the Mechanism of Flame Propagation in Tube [In Chinese]. Ph.D. Thesis, China University of Mining and Technology, Xuzhou, China, April 2003.
7. Rubtsov, N.M.; Seplyarskii, B.S. On the nature of an upper concentration limit of flame propagation in an H₂ + air mixture. *Mendeleev Commun.* **2009**, *19*, 227–229.
8. Zhang, X.Q.; Lei, Y.; Wang, B.R.; Wang, Y.; Wei, M.G. Turbulence in laminar premixed V-flames. *Sci. China* **2003**, *6*, 574–580.
9. Oh, K.H.; Kim, H.; Kim, J.B. A study on the obstacle induced variation of the gas explosion characteristics. *J. Loss Prev. Process Ind.* **2001**, *6*, 597–602.
10. Patel, S.N.; Jarvis, S.; Ibrahim, S.S. An experimental and numerical investigation of premixed flame deflagration in a semiconfined explosion chamber. *Proc. Combust. Inst.* **2002**, *29*, 1849–1854.
11. Le, H.; Nayak, S.; Mannan, M.S. Upper flammability limits of hydrogen and light hydrocarbons in air at subatmospheric pressures. *Ind. Eng. Chem. Res.* **2012**, *51*, 9396–9402.
12. Xiao, H.H.; Makarov, D.; Sun, J.H.; Molkov, V. Experimental and numerical investigation of premixed flame propagation with distorted tulip shape in a closed duct. *Combust. Flame* **2012**, *159*, 1523–1538.
13. Clanet, C.; Searby, G. On the “tulip flame” phenomenon. *Combust. Flame* **1996**, *105*, 225–238.
14. Bychkov, V.; Akkerman, V.; Fru, G.; Petchenko, A.; Eriksson, L.E. Flame acceleration in the early stages of burning in tubes. *Combust. Flame* **2007**, *150*, 263–276.
15. Rankin, D.D.; Mecann, M.A. Overpressures from nondetonating, baffle-accelerated turbulent flames in tubes. *Combust. Flame* **2000**, *120*, 504–514.
16. Di Sarli, V.; Di Benedetto, A.; Russo, G. Large Eddy Simulation of transient premixed flame-vortex interactions in gas explosions. *Chem. Eng. Sci.* **2012**, *71*, 539–551.
17. Shelkin, K.I. Influence of tube non-uniformities on the detonation ignition and propagation in gases. *Exp. Theor. Phys.* **1940**, *10*, 823–827.
18. Bychkov, V.; Valiev, D.; Eriksson, L.E. Physical mechanism of ultrafast flame acceleration. *Phys. Rev. Lett.* **2008**, *101*, 164501:1–164501:4.
19. Akkerman, V.; Bychkov, V.; Petchenko, A.; Eriksson, L.E. Accelerating flames in cylindrical tubes with nonslip at the walls. *Combust. Flame* **2006**, *145*, 206–219.

20. Bychkov, V.; Petchenko, A.; Akkerman, V.; Eriksson, L.E. Theory and modeling of accelerating flames in tubes. *Phys. Rev. E* **2005**, *72*, 046307:1–046307:10.
21. Park, D.J.; Green, A.R.; Lee, Y.S.; Chen, Y.C. Experimental studies on interactions between a freely propagating flame and single obstacles in a rectangular confinement. *Combust. Flame* **2007**, *150*, 27–39.
22. Di Sarli, V.; di Benedetto, A.; Russo, G. Using Large Eddy Simulation for understanding vented gas explosions in the presence of obstacles. *J. Hazard. Mater.* **2009**, *169*, 435–442.
23. Kirkpatrick, M.P.; Armfield, S.W.; Masri, A.R.; Ibrahim, S.S. Large Eddy Simulation of a propagating turbulent premixed flame. *Flow Turbul. Combust.* **2003**, *70*, 1–19.
24. Di Sarli, V.; di Benedetto, A.; Russo, G.; Jarvis, S.; Long, E.J.; Hargrave, G.K. Large Eddy Simulation and PIV measurements of unsteady premixed flames accelerated by obstacles. *Flow Turbul. Combust.* **2009**, *83*, 227–250.
25. Mardani, A.; Tabejamaat, S.; Mohammadi, M.B. Numerical study of the effect of turbulence on rate of reactions in the MILD combustion regime. *Combust. Theory Model.* **2011**, *15*, 753–772.
26. Sadiki, A.; Maneshkarimi, M.R.; Chrighui, M. Towards an optimization of turbulence effects on heat and mass transfer in evaporating and reacting gas turbine sprays. In *Proceedings of the 50th ASME Turbo-Expo*, Reno, NV, USA, 6–9 June 2005.
27. Salzano, E.; Marra, F.S.; Russo, G.; Lee, J.H.S. Numerical simulation of turbulent gas flames in tubes. *J. Hazard. Mater.* **2002**, *95*, 233–247.
28. Park, J.W.; Oh, C.B. Flame structure and global flame response to the equivalence ratios of interacting partially premixed methane and hydrogen flames. *Int. J. Hydrog. Energy* **2012**, *37*, 7877–7888.
29. Barlow, R.S. Laser diagnostics and their interplay with computations to understand turbulent combustion. *Proc. Combust. Inst.* **2007**, *31*, 49–75.
30. Kersten, C.; Forster, H. Investigation of deflagrations and detonations in pipes and flame arresters by high-speed framing. *J. Loss Prev. Process Ind.* **2004**, *17*, 43–50.
31. Chen, X.F.; Sun, J.H.; Liu, Y. Microstructure of premixed propane/air flame in the transition from laminar to turbulent combustion. *Chin. Sci. Bull.* **2007**, *52*, 685–691.
32. Wu, M.H.; Burke, M.P.; Son, S.F.; Yettera, R.A. Flame acceleration and the transition to detonation of stoichiometric ethylene/oxygen in microscale tubes. *Proc. Combust. Inst.* **2007**, *31*, 2429–2436.
33. Torgny, E.; Carlsson, R.M. Combination of Schlieren and pulsed TV holography in the study of a high-speed flame jet. *Opt. Lasers Eng.* **2006**, *44*, 535–554.
34. Kuzuu, K.; Ishii, K.; Kuwahara, K. Numerical simulation of premixed flame propagation in a closed tube. *Fluid Dyn. Res.* **1996**, *3*, 165–182.
35. McIntosh, A.C. The linearised response of the mass burning rate of a premixed flame to rapid pressure changes. *Combust. Sci. Tech.* **1993**, *91*, 329–346.
36. Strehlow, R. *Combustion Fundamentals*; McGraw-Hill: New York, NY, USA, 1984.
37. Konga, B.N.; Fernandez, G.; Guillard, H.; Larrouturou, B. Numerical investigations of the tulip flames instability-comparisons with experimental results. *Combust. Sci. Tech.* **1992**, *87*, 69–89.
38. Guenoche, H. *Nonsteady Flame Propagation*; Oxford: New York, NY, USA, 1964.

39. Patnaik, G.; Kailasanath, K. Numerical simulation of the extinguishment of downward propagating flames. In *Proceedings of the 24th International Symposium on Combustion*, Sydney, Australia, 5–10 July 1992.
40. Bychkov, V.; Liberman, M.A. Dynamics and stability of premixed flames. *Phys. Rep.* **2000**, *325*, 116–237.
41. Modestov, M.; Bychkov, V.; Betti, R.; Eriksson, L.E. Bubble velocity in the nonlinear Rayleigh–Taylor instability at a deflagration front. *Phys. Plasmas* **2008**, *15*, 042703:1–042703:12.
42. Bychkov, V.; Modestov, M.; Akkerman, V.; Eriksson, L.E. The Rayleigh–Taylor instability in inertial fusion, astrophysical plasma and flames. *Plasma Phys. Control. Fusion* **2007**, *49*, B513–B520.
43. Davis, S.G.; Quinard, J.; Searby, G. Markstein numbers in counterflow, methane- and propane-air flames: A computational study. *Combust. Flame* **2002**, *130*, 123–136.
44. Akkerman, V.; Bychkov, V. Velocity of weakly turbulent flames of finite thickness. *Combust. Theory Model.* **2005**, *9*, 323–351.
45. Xu, S.L.; Zhang, H.J.; Yue, P.T. Study on properties of pressure waves generated by steady flames in a duct. *J. China Univ. Sci. Tech.* **2000**, *4*, 387–392.
46. Bychkov, V.; Liberman, M. Comment on “The influence of hydrodynamic instability on the structure of cellular flames”. *Phys. Fluids* **2002**, *14*, 2024–2025.
47. Petchenko, A.; Bychkov, V.; Akkerman, V. Flame-sound interaction in tubes with nonslip walls. *Combust. Flame* **2007**, *149*, 418–434.
48. McIntosh, A.C. Pressure disturbances of different length scales interacting with conventional flames. *Combust. Sci. Tech.* **1991**, *75*, 287–309.
49. Bychkov, V.; Akkerman, V.; Valiev, D.; Law, C.K. Influence of gas compression on flame acceleration in channels with obstacles. *Combust. Flame* **2010**, *157*, 2008–2011.
50. Valiev, D.; Bychkov, V.; Akkerman, V.; Eriksson, L.E. Different stages of flame acceleration from slow burning to Chapman-Jouguet deflagration. *Phys. Rev. E* **2009**, *80*, 036317:1–036317:11.
51. Bychkov, V.; Akkerman, V.; Valiev, D.; Law, C.K. Role of compressibility in moderating flame acceleration in tubes. *Phys. Rev. E* **2010**, *81*, 026309:1–026309:9.
52. Wang, H.; Ge, L.M.; Deng, J. Comparison of explosion characteristics of ignitable gases in confined space. *J. China Coal Soc.* **2009**, *2*, 218–223.